Active shock absorber control in humanoid robot falls with nonlinear optimization on a reduced dynamics model

Vincent Samy[1], Karim Bouyarmane[2] and Abderrahmane Kheddar[3,1]

***Abstract*— We propose a reduced-model-based analytic approach to active shock absorption by a falling humanoid robot at impact. We model the segment between the contact point at impact and the impacting limb extremity attached to the torso or waist of the humanoid robot as a one degree-of-freedom linear mass-spring-damper system. By mapping the joint angle limits and torque limits of the joints in the impacting limb to a corresponding position limit and force limit in the reduced model, we formulate a nonlinear optimization problem to find an admissible pair of parameters of the reduced model (stiffness, damping) that prevents the model from violating the constraints before reaching a steady state rest. The nonlinear constraints are analytically derived using symbolic computation tools and then numerically solved with off-the-shelf nonlinear optimization solver. The reduced model trajectories are then mapped back on the full body of the humanoid robot and illustrated on the HRP-4 robot in simulation.**

I. Introduction

Reduced-dynamics models, such as the center-of-mass (CoM) and multi-dimensional mass-spring-dampers, proved to be extremely efficient in capturing the dominant behavior of complex dynamical systems, among which humanoid robots. For example, the CoM and related centroidal dynamics are used to design various strategies for dynamic walking, see [1], [2]. The linear inverted pendulum (LIP) model can be cited as one of the most popular in the humanoid robotics research community since many years [3]. The CoM model enhanced by a spring along the massless CoM/Center of Pressure point system (spring-loaded inverted pendulum, or SLIP) is used to generate behaviors beyond walking, e.g. jumping and running [4], [5], [6]. Reduced CoM models were extended to generate multi-contact motions, e.g. [7], [8]. Mass-spring-damper models have also been used as nominal desired impedance or admittance at the contact space [9]. There are of course many other variants of reduced-dynamics models and their usages in robotics.

In our previous work, we have addressed humanoid falling using locally linearized control to comply with post-impact dynamics using task-space quadratic programming (QP) control formalism [10], [11]. The idea [12] is to reshape the humanoid posture so as to meet the impacts at contact positions that maximize compliance by active change of the actuators Proportional-Derivative (PD) gains. Recently in [13], we showed that the actuator gain parameters can also be integrated as decision variables in the QP controller, and can thus be computed together with the state acceleration and contact forces. However, a problem that still needed to be solved was the computation of motor PD gains using a prediction of the system over a horizon of time (preview control) to ensure that the structural limits of the robot (torque limits, joint limits) are not reached during the whole post-impact phase, until the system comes to a rest.

In this paper, we propose to study a mass-spring-damper reduced-dynamics model applied to the situation of falling for a humanoid robot, to be used in a two-stage approach followed by whole-body QP control, similarly to what is well established in dynamic walking. The idea of the reduced-dynamics model is to emulate a shock absorber on the impacting limbs of the robot (see Fig. 1).

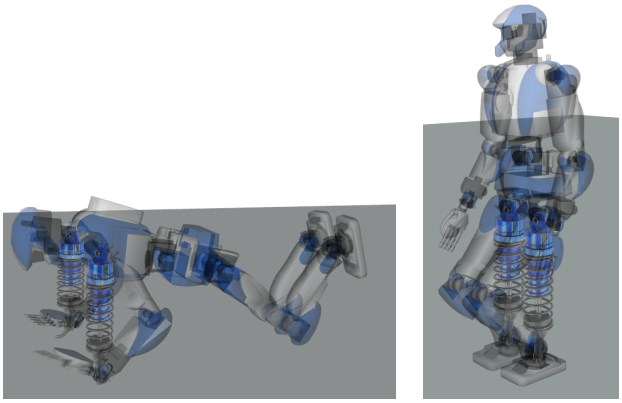

(a) Landing on arms. (b) Landing on legs.

Fig. 1: Shock-absorber reduced-dynamics-model representation in two different landing configurations.

To this end, we present a detailed analysis of the parameter tuning of a one degree-of-freedom (1 dof) mass-spring-damper system to serve as a model-preview controller for post-impact trajectory generation of humanoid whole-body motion. We analytically derive the constraints on the stiffness and damping parameters of the reduced model and formulate a nonlinear optimization problem to solve for them. Once the parameters of the model are obtained, the corresponding trajectory is tracked by the robot in the post-impact phase using a whole-body controller.

The rest of the paper is organized as follows. Section II presents the reduced model and the analytical study that leads to the nonlinear optimization problem on its stiffness and damping parameters. Section III shows results obtained in simulation on full humanoid robot falling in different

[1]CNRS-University of Montpellier LIRMM, Interactive Digital Human group, France.

[2]Université de Lorraine, Inria, CNRS, Loria UMR 7503, Larsen team, France.

[3]CNRS-AIST Joint Robotics Laboratory, UMI3218/RL, Japan.

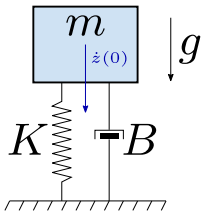

Fig. 2: Mass-spring-damper system.

configurations. Finally, Section IV concludes the paper with a discussion on limitations, possible improvement, and future work suggestions.

II. Analytical resolution

Let us consider the system in Fig. 2. The analytical solution for the motion of this system comes from the standard resolution of the well-studied second order linear differential equation:

$$\begin{aligned} & m\ddot{z}(t) - Ke(t) - B\dot{e}(t) + mg = 0\,, \\ \Leftrightarrow\ & m\ddot{z}(t) - K(z^{\text{ref}} - z(t)) - B(\dot{z}^{\text{ref}} - \dot{z}(t)) + mg = 0\,, \end{aligned} \tag{1}$$

where m is the mass of the system, $z(t)$ is the position of the mass at time t, g the gravity and K, B the gains that we want to compute to satisfy the constraints that will be mapped from the torque limit and joint angle limits of the full system. This equation can also be interpreted as a PD controller of a linear motor supporting a mass m under the gravity g. In such case, z^{ref} is the desired position which is set to the position just before impact $q^{-}(0)$ and $\dot{z}^{\text{ref}}$ is always 0.

It is well known that when solving for $z(t)$, three cases are distinguished. An under-damped solution occurs if $B^2 < 4mK$. The system keeps oscillating at its natural frequency. The critically damped solution occurs when $B^2 = 4mK$. It is the fastest way to reach the z^{ref} position without oscillating. The last solution is the over-damped one when $B^2 > 4mK$. This also leads to reaching z^{ref} without oscillating, but over a longer time.

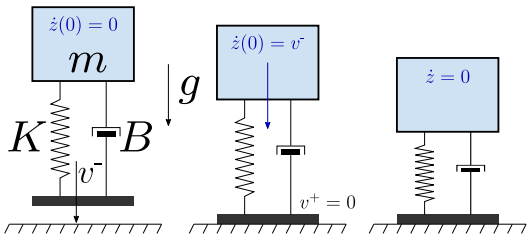

Fig. 3: Phases of landing and impact of the reduced model. The left figure represents the system just before impact at time $t = 0^{-}$, the velocity of the base is v^{-} and the joint velocity is 0 (velocity of the mass relative to the base). The middle figure represents the system just after impact at $t = 0^{+}$. The right figure represents the system at the time of maximum amplitude $t = t^{\text{ma}}$.

Given a solution of Eq. (1) that depends on the parameters K and B, our objective is to find admissible values of these parameters such that:

- **joint limit constraint:** a position limit constraint is satisfied on $z(t)$ (e.g. preventing the mass from colliding with the ground after the impact, or equivalently reaching a maximum compression limit),
- **torque limit constraint:** a force limit constraint is satisfied on $K(z^{\text{ref}} - z(t)) + B(\dot{z}^{\text{ref}} - \dot{z}(t))$ (the impact force generated by the spring recoil should be kept below a safety threshold when possible),
- the system converges to zero velocity.

The above constraints capture in the reduced model the full-body constraints on both joints angle and torques limits.

Based on these constraints, we choose to search for over-damped solutions. The reasons behind this choice are that: 1) we want to avoid unnecessary oscillations of the reduced model which, if mapped to the whole-body, will reproduce an undesired shaking behavior of the system after impact; and 2) We are not interested in critically converging to z^{ref}, as long as we reach a rest steady state over time. Hence, we solve Eq. (1) assuming $B^2 > 4mK$. We will see later that this is not a limiting assumption in terms of finding a solution whenever the solution set is nonempty.

Note that we do not consider an explicit velocity constraint in the formulation, as during the entire post-impact phase, the system is only decelerating (slowing down) due to the dissipation of energy through the damping, so the constraint would only be effective if written on the initial velocity. However, the latter is an input to the problem over which we have no direct control. Therefore, the post-impact initial velocity might or might not cross the velocity limit if it was to be set. For these reasons, we do not explicitly formulate a velocity constraint.

Solving the differential equation Eq. (1) for z as a function

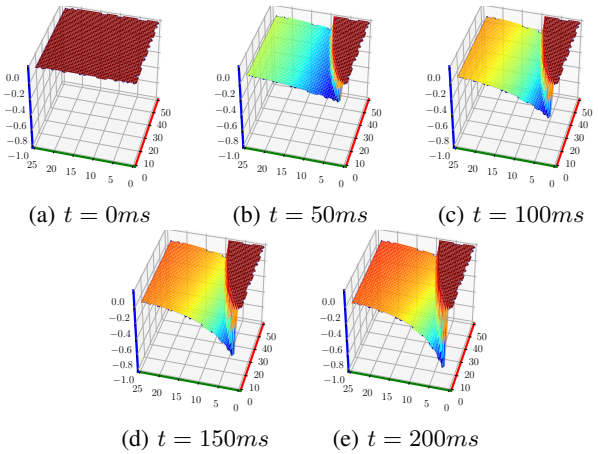

(a) $t = 0ms$ (b) $t = 50ms$ (c) $t = 100ms$

(d) $t = 150ms$ (e) $t = 200ms$

Fig. 4: Evolution of the position z for a given set ($K \in [0..50]$, $B \in [0..25]$). The red axis is the stiffness K in N.m^{-1}, the green axis is the damping B in N.s.m^{-1} and the blue axis is the position z in m.

of t, with K and B as parameters, leads to:

$$z(t,K,B) = \frac{e^{-\frac{1}{2m}(B-\sqrt{\gamma})t}(Bg + 2K\dot{z}(0) + \sqrt{\gamma}g)m}{2\sqrt{\gamma}K} - \frac{e^{-\frac{1}{2m}(B+\sqrt{\gamma})t}(Bg - 2K\dot{z}(0) - \sqrt{\gamma}g)m}{2\sqrt{\gamma}K} + \frac{Kz(0) - mg}{K}, \quad (2)$$

with $\gamma = B^2 - 4Km$.

In the following, for the sake of readability and in order to reduce the size of the symbolic expressions, but without loss of generality, we set example numerical values to the initial conditions and to the mass of the system (all the developments can be kept with their symbolic expressions):

$$\begin{cases} m = 1\,, \\ g = 9.81\,, \\ z(0) = 0\,, \\ \dot{z}(0) = \text{-}5\,. \end{cases} \quad (3)$$

The derivations and reasoning to follow are still valid for any other numerical values corresponding to the specific robot and falling conditions at hand. Initializing the velocity to a value different from zero simulates a falling system state just after an impact. Suppose the system is impacting with a net velocity $v^- = \text{-}0.5\,\text{ms}^{\text{-}1}$ (external floating-base velocity) and $\dot{z}^-(0) = 0\,\text{ms}^{\text{-}1}$ (internal joint velocity) and that the impact is inelastic (no bounce), the remaining velocity in the joint post-impact is then $\dot{z}^+(0) = \text{-}5\,\text{ms}^{\text{-}1}$, see Fig. 3.

With the numerical values (3), $z(t,K,B)$ in (2) becomes:

$$z(t,K,B) = \frac{e^{-\frac{1}{2}(B-\sqrt{\gamma})t}(\text{-}10K + 9.81(B+\sqrt{\gamma})}{2\sqrt{\gamma}K} - \frac{e^{-\frac{1}{2}(B+\sqrt{\gamma})t}(10K + 9.81(B-\sqrt{\gamma})}{2\sqrt{\gamma}K} - \frac{9.81}{K}, \quad (4)$$

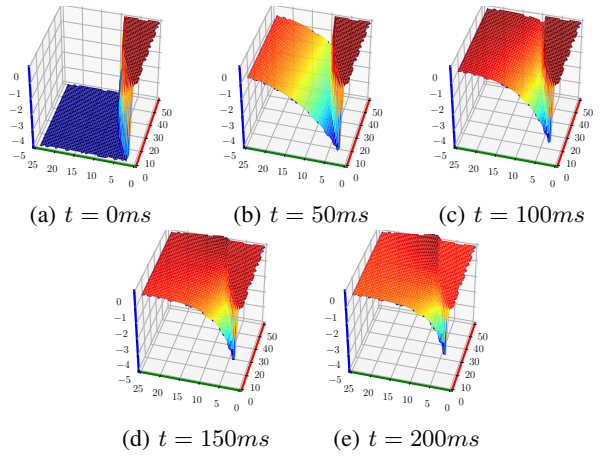

(a) $t = 0ms$ (b) $t = 50ms$ (c) $t = 100ms$

(d) $t = 150ms$ (e) $t = 200ms$

Fig. 5: Evolution of the velocity $\dot{z}$ for a given set ($K \in [0..50]$, $B \in [0..25]$). The red axis is the stiffness K in N.m$^{\text{-}1}$, the green axis is the damping B in N.s.m$^{\text{-}1}$ and the blue axis is the velocity $\dot{z}$ in m.s$^{\text{-}1}$.

with $\gamma = B^2 - 4K$ (we recall that $\gamma > 0$).

A 3D time-evolution representation of z as function of K and B can be represented, this is illustrated in Fig. 4.

Taking the time-derivative of $z(t,K,B)$ gives us the joint velocity:

$$\dot{z}(t,K,B) = \frac{(\text{-}B + \sqrt{\gamma})e^{-\frac{1}{2}(B-\sqrt{\gamma})t}(\text{-}10K + 9.81(B+\sqrt{\gamma}))}{4\sqrt{\gamma}K} - \frac{(\text{-}B - \sqrt{\gamma})e^{-\frac{1}{2}(B+\sqrt{\gamma})t}(10K + 9.81(B-\sqrt{\gamma}))}{4\sqrt{\gamma}K}. \quad (5)$$

The 3D time-evolution of $\dot{z}$ as a function of K and B can also be visualized (Fig. 5).

Lastly, from z and $\dot{z}$, we can compute the joint force (spring force) with respect to time and as a function of K and B (Eq. (6) and Fig. 6).

$$f(t,K,B) = K(z^{\text{ref}} - z(t,K,B)) - B\dot{z}(t,K,B) = \text{-}\frac{(2.5B^2 - 5K - 4.905B + (4.905 - 2.5B)\sqrt{\gamma})e^{-\frac{1}{2}(B-\sqrt{\gamma})t}}{\sqrt{\gamma}} - \frac{(\text{-}2.5B^2 + 5K + 4.905B + (4.905 - 2.5B)\sqrt{\gamma})e^{-\frac{1}{2}(B+\sqrt{\gamma})t}}{\sqrt{\gamma}} + 9.81\,. \quad (6)$$

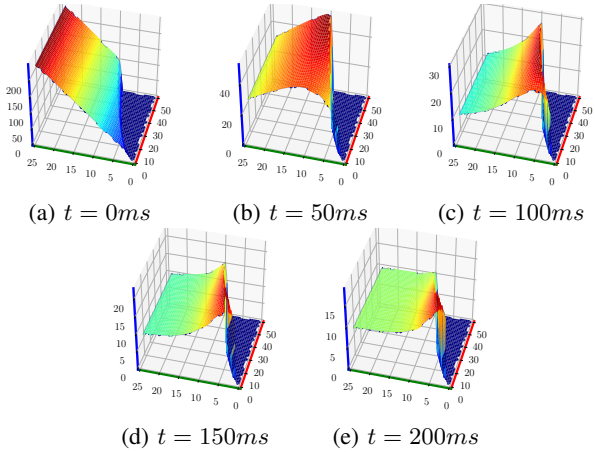

(a) $t = 0ms$ (b) $t = 50ms$ (c) $t = 100ms$

(d) $t = 150ms$ (e) $t = 200ms$

Fig. 6: Evolution of the force f for a given set ($K \in [0..50]$, $B \in [0..25]$). The red axis is the stiffness K in N.m$^{\text{-}1}$, the green axis is the damping B in N.s.m$^{\text{-}1}$ and the blue axis is the force f in N.

The joint limit and force limit constraints can be respectively written from the expressions (4) and (6) as

$$\forall t > 0 \quad \underline{z} \leq z(t,K,B) \leq \overline{z}\,, \quad (7)$$

$$\forall t > 0 \quad \underline{f} \leq f(t,K,B) \leq \overline{f}\,, \quad (8)$$

where $\underline{z}$, $\overline{z}$, $\underline{f}$, $\overline{f}$ are the lower and upper bounds of the reduced system position and force mapped from the joint limit constraints and torque limits constraints of the considered robot impacting limb (see Section III).

The projection of the joint limit constraint and the torque limit constraint on the K-B plane through time is visualized in Fig. 7. The joint limit visualization is obtained by intersecting the 3D time-evolution plot of $z(t, K, B)$ with the plane $z = \underline{z}$, while the force limit constraint visualization is obtained by intersecting the 3D time-evolution plot of $f(t, K, B)$ with the plane at $f = \overline{f}$ (the reason why only one side of these two constraints is relevant is explained below). By analyzing these time visualizations, we can substitute the time-continuous constraints (7) and (8) with fixed time constraints.

First, we can define the maximum amplitude time t^{ma} as the time at which the velocity reaches 0. Solving for Eq. (5) $= 0$ with K and B as parameters using a symbolic computation software (e.g. Maple), we get:

$$t^{\text{ma}} = \frac{\ln\left(-\frac{4905B-2500K-9623.61}{1250B^2-1250B\sqrt{\gamma}-2500K-4905B+4905\sqrt{\gamma}+9623.61}\right)}{\sqrt{\gamma}}. \tag{9}$$

This equation is stiffness-dependant and damping-dependant. The **joint limit constraint** can then be captured by:

$$\underline{z} \leq z(t = t^{\text{ma}}, K, B) \leq \overline{z}. \tag{10}$$

Secondly, we observe that the force limit can be reached in three main ways: i) high damping force when having high velocity; ii) high stiffness force when having high position error; iii) a mix of the two. In this study, we are interested in impacts involving a relatively short post-impact distance traveled between initial position and the limit, and high post-impact velocity coming from the fall. Placing ourselves in these conditions, the force maximum value is more likely to come from the damping of the velocity and not from the stiffness related to the distance. And since we will only decelerate the system, we consider that the maximum force is reached at $t = 0^+$ (impact force). The **torque limit constraint** (here a force limit constraint) thus writes:

$$\underline{f} \leq f(t = 0^+, K, B) \leq \overline{f}. \tag{11}$$

Of course, it is necessary to confirm this latter assumption once the $t \mapsto f(t)$ trajectory is derived with the computed values of K and B. This is the case in Fig. 7b.

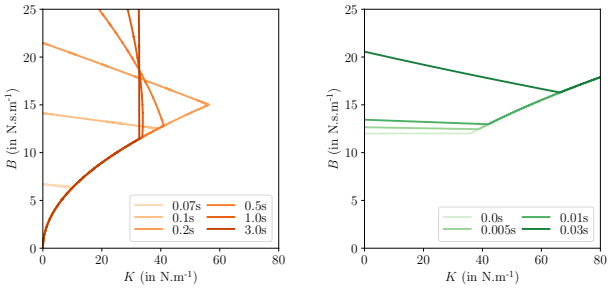

(a) Joint limit projection. (b) Force limit projection.

Fig. 7: Projection of the joint limit and the force limit on the K-B plane for different time with $\underline{z}$ = -0.3m and $\overline{f}$ = 60N.

As only the over-damped behavior is taken into account, a third constraint, the **over-damped system constraint**, is added to the above joint limit and torque limit constraints.

$$4K - B^2 < 0. \tag{12}$$

The problem we have formulated up to this point thus reduces to the following system of inequalities:

$$\text{find } K, B \tag{13}$$

$$\text{such that } \begin{cases} \underline{z} \leq z(t = t^{\text{ma}}, K, B) \leq \overline{z} \\ \underline{f} \leq f(t = 0^+, K, B) \leq \overline{f} \\ 4K - B^2 < 0 \end{cases} \tag{14}$$

This is a system of nonlinear inequalities, as the constraints (10)–(12) are nonlinear inequalities in K and B, of which we have derived the analytical expressions throughout this section using symbolic computation tools.

To solve our system of nonlinear inequalities, we formulate it as the system of constraints of a nonlinear constrained optimization problem in K and B, with an arbitrary convex cost function, e.g. minimizing $K^2 + B^2$:

$$\min_{K,B} \quad K^2 + B^2 \tag{15}$$

$$\text{such that } \begin{cases} \underline{z} \leq z(t = t^{\text{ma}}, K, B) \leq \overline{z} \\ \underline{f} \leq f(t = 0^+, K, B) \leq \overline{f} \\ 4K - B^2 < 0 \end{cases}$$

that finds the minimum norm solution for (K, B) satisfying the system of nonlinear inequality constraints.

We use the Matlab software to compute the solution of this optimization problem (The use of other non-linear optimization frameworks that are robotics-applications optimized, such as [14], is possible). The result is shown in Fig. 8. In this example, the impulse happens at the time $t_0 = 0$ such that at t_0^- the velocity is zero and at t_0^+ the velocity is -5m.s^{-1} and $z(0) = 0$, $\underline{z}$ = -0.5, $\overline{f}$ = 60.

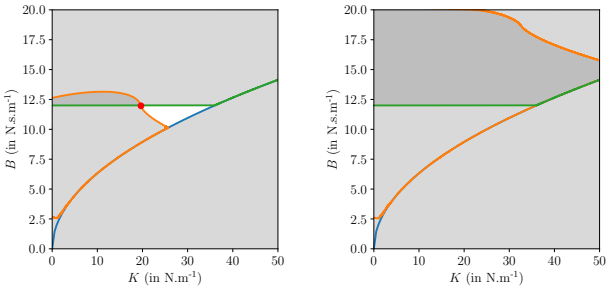

(a) Solution region ($\underline{z}$ = -0.5) (b) No solution ($\underline{z}$ = -0.3)

Fig. 8: Computation of the solution region depending on the problem constraints in the K-B domain. The blue curve represents Eq. (12), the green curve Eq. (11) and the orange curve Eq. (10). The set of admissible solutions of the system of nonlinear inequalities is the white region. The red dot is the particular solution of the the nonlinear optimization problem.

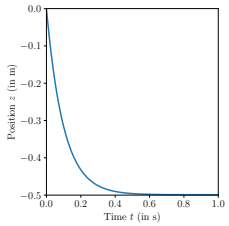

(a) Evolution of $z(t)$.

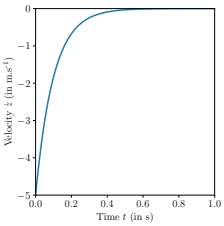

(b) Evolution of $\dot{z}(t)$.

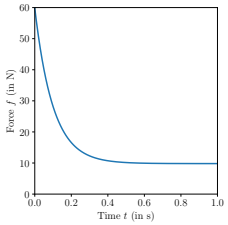

(c) Evolution of $f(t)$.

Fig. 9: Evolution of the different joint parameters through time. The system reaches the joint limit without crossing it and after around 0.5s it is completely stopped.

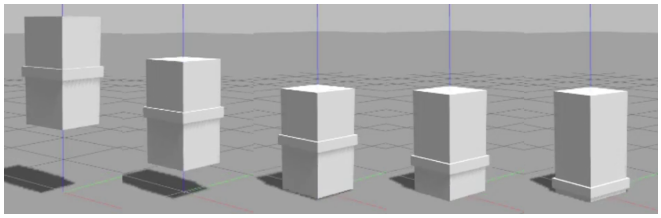

(a) 1-dof system simulation.

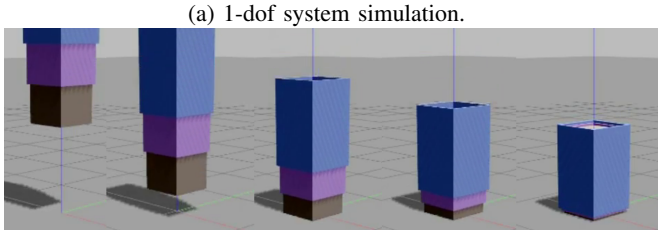

(b) 2-dof system simulation.

Fig. 10: low-dimensional systems simulations.

When the joint limit is not too close to the current position (Fig. 8a), we are able to find a set of solutions that satisfy all the constraints (Fig. 9). However, if the joint limit is set to 0.3 instead of 0.5 (much closer to the current position) as in Fig. 8b, no solution can be found, as the solution set is empty. The latter situation can also occur in falling conditions from which it is impossible for the robot to safely recover (e.g. dropping from a high altitude, impacting with very high velocity).

III. Results

The accompanying video shows simulations that were realized based on the presented approach, first with low-dimensional systems (matching the studied model) and on a full humanoid robot HRP-4.

Fig. 10a is a trivial application of the method on a 1-dof system, in this case the reduced-model corresponds to the full model.

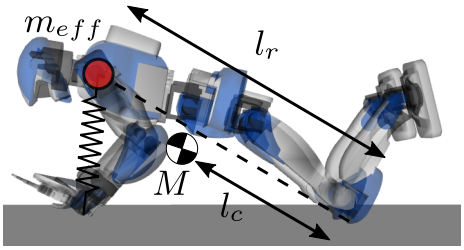

Fig. 11: Effective mass computation.

Fig. 10b shows an application to a 2-dof system with two prismatic joints. The maximum force $\overline{f}$ is the sum of the maximum forces of the two linear actuators, and the minimum position $\underline{z}$ is obtained when the two joints are put at their position limits.

In both examples, we obtain a perfect realization of the desired behavior in simulation, after both systems reach the ground with an impact velocity of $v^- = -5\text{ms}^{-1}$.

Figs. 12 and 13 show falling motions of the HRP-4 robot, controlled based on the reduced-model approach illustrated in Fig. 1. The reduced-model analysis is used to generate trajectories for the limb extremity attached to torso (arms) or to the waist (legs), and these trajectories are tracked in the post impact phase with a whole-body controller.

In these two cases, the limit position of the reduced model $\underline{z}$ is obtained from forward kinematics of the limb of interest when all the joints of that limb are put in their respective joint limits:

$$\underline{z} = \text{FK}^{\text{limb}}(q^{\text{limb}}_{\text{limit}}), \tag{16}$$

where FK^{limb} denotes the forward kinematics function of the limb and $q^{\text{limb}}_{\text{limit}}$ the configuration of the limb at its limits (here limb $\in \{\text{arm}, \text{leg}\}$). However, it is only an approximation, since FK^{limb} is generally a nonlinear mapping. This example shows that obtaining the exact bounds on the reduced model range of motion (i.e. the compression limit of the reduced system) from the robot joint limits and the kinematics is not trivial. We discuss other possible methods in the discussion section (Section IV). For the limit force of the reduced model, it can be obtained in first approximation from the pseudo inverse of the Jacobian transpose applied on the torque limits of the limb, or obtained exactly by using the force polytope analysis detailed in [15], that accounts for both torque limits in the limb and friction limits at the contact.

As for the effective mass of the reduced model in case of landing on the arms, we use the reasoning illustrated in Fig. 11. Modeling the part of the robot between the knee and the arm as an inverted pendulum rod, the effective mass can be defined as the point mass localized at the extremity of the rod that has the same moment around the center-of-pressure (CoP) of the rod as the total gravity force applied at the CoM, i.e.

$$Mgl_c\cos(\theta) = m_{\text{eff}}gl_r\cos(\theta), \tag{17}$$

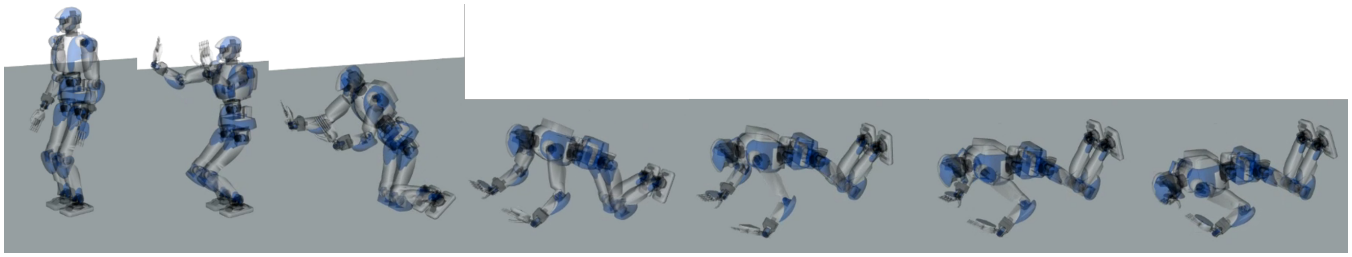

Fig. 12: Front fall screenshots from the accompanying video.

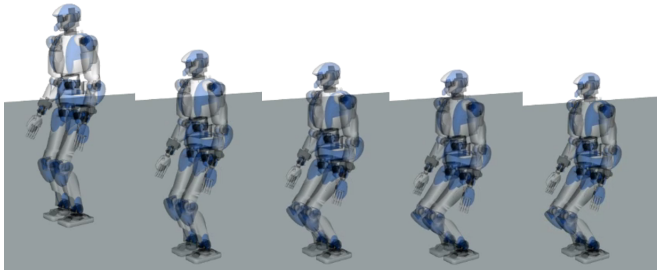

Fig. 13: Leg fall screenshots from the accompanying video.

where M is the mass of the rod (mass of the robot between the knee and the arm), l_c the distance of the CoM of the rod from its CoP at the knee, l_r the total length of the rod (distance between the effective mass and the CoP), and θ the angle between the rod and and ground. Therefore, we have:

$$m_{\text{eff}} = M\frac{l_c}{l_r}\,. \tag{18}$$

The impact velocities for the arm landing and leg landing falls were respectively measured at $v^- = -3\text{ms}^{-1}$ and $v^- = -1.47\text{ms}^{-1}$. In Fig. 12, the particular posture that the robot adopts just before it starts falling is generated by applying the method presented in our previous work on non-singular falls and optimal falling postures [12], [13].

IV. Conclusion and Discussion

We presented a study on a reduced model to capture the dynamics of active post-impact shock absorption when a humanoid robot falls and collides with the environment.

The analysis of the system allowed us to find the stiffness and damping parameters (K, B) of the reduced model that satisfy, when possible, the structural limits that are the joint limits and torque limits mapped onto a position limit and force limit on the reduced model. This reduced-model approach results in trajectories that are subsequently tracked by a whole-body controller, simulating the behavior needed by the humanoid to realize active impact compliance following the model.

As discussed in Section III, a general exact mapping from the limbs joint limits of a humanoid robot to the bounds on the range of motion of the corresponding reduced models can be difficult to obtain. A good approximation and practical method consisted in using forward kinematics and reachable space computation of the point corresponding to the attachment of the mass considering the contact constraint. This is the method we used in our examples. An alternative method would be to represent the kinematic tree structure of the humanoid as a deformable structure (through a rigidity matrix [16]) with repulsive potential fields at the joint limits, and use computer graphics animation techniques (such as a virtual force pulling the reduced-model's attachment point along the gravity until equilibrium is reached) to compute the desired bounds iteratively. This can be obtained with very fast simple computations. We plan to investigate this technique in future work.

Our analysis highlighted situations in which no solution exists (when the solution set on (K, B) is empty), due to extreme falling conditions for example (high impact velocity) or very limiting bounds. In these situations, the proposed approach is unsuccessful and the model appears to be no longer valid to propose a practical damage-reduction solution. Future work will investigate what alternative models can be used to deal with these extreme situations.

Moreover, other limiting situations in which a constant (K, B) solution does not fit in the constraint region throughout the time can also occur. It can be overcome in future work by seeking for time-varying $(K(t), B(t))$. We can optimize for those with trajectory optimization techniques using basis-functions parameterization (e.g. splines).

The approach in this work was specifically designed for position-controlled robots, and applied in simulation by tracking the desired trajectories by a whole-body controller with high motor PD gains. We plan in the future to combine this work with our previous work on low-level motor PD gain adaptation [13] to realize the tracking of the trajectories with lower adaptive motor PD gains.

Finally, we plan to extend the analysis proposed here to directly tune the low-level motor PD gains of the joints by using a multi-dof system modeling the compliance with a torsional spring-damper behavior at each joint.

ACKNOWLEDGMENT

This work is supported in parts from grants of the COMANOID EU H2020 project www.comanoid.eu and of the Japan Society for Promotion of Sci- ence (JSPS) Grant-in-Aid for Scientific Research, Kakenhi B No. 16H02886

References

[1] D. E. Orin, A. Goswami, and S.-H. Lee, "Centroidal dynamics of a humanoid robot," *Autonomous Robots*, vol. 35, no. 2, pp. 161–176, Oct 2013. [Online]. Available: https://doi.org/10.1007/s10514-013-9341-4

[2] P.-B. Wieber, S. Kuindersma, and R. Tedrake, "Modeling and control of legged robots," in *Springer Handbook of Robotics*, 2nd ed., B. Siciliano and O. Khatib, Eds. Springer Berlin Heidelberg, 2015, ch. 48.

[3] S. Kajita, F. Kanehiro, K. Kaneko, K. Fujiwara, K. Harada, K. Yokoi, and H. Hirukawa, "Biped walking pattern generation by using preview control of zero-moment point," in *Robotics and Automation, 2003. Proceedings. ICRA'03. IEEE International Conference on*, vol. 2. IEEE, 2003, pp. 1620–1626.

[4] H. Geyer, A. Seyfarth, and R. Blickhan, "Compliant leg behaviour explains basic dynamics of walking and running," *Proceedings of the Royal Society of London B: Biological Sciences*, vol. 273, no. 1603, pp. 2861–2867, 2006.

[5] I. Mordatch, M. de Lasa, and A. Hertzmann, "Robust physics-based locomotion using low-dimensional planning," *ACM Transactions on Graphics (SIGGRAPH)*, vol. 29, no. 3, 2010.

[6] P. M. Wensing and D. E. Orin, "3D-SLIP steering for high-speed humanoid turns," in *IEEE/RSJ International Conference on Intelligent Robots and Systems*, 2014, pp. 4008–4013.

[7] I. Mordatch, E. Todorov, and Z. Popović, "Discovery of complex behaviors through contact-invariant optimization," *ACM Transactions on Graphics (SIGGRAPH)*, vol. 31, no. 4, p. 43, 2012.

[8] H. Audren, J. Vaillant, A. Kheddar, A. Escande, K. Kaneko, and E. Yoshida, "Model preview control in multi-contact motion-application to a humanoid robot," in *IEEE/RSJ International Conference on Intelligent Robots and Systems*, Sept 2014, pp. 4030–4035.

[9] N. Hogan, "Impedance control: An approach to manipulation: Part i—theory," *Journal of Dynamic Systems, Measurement, and Control*, vol. 107, no. 1, pp. 1–7, 03 1985. [Online]. Available: http://dx.doi.org/10.1115/1.3140702

[10] J. Vaillant, K. Bouyarmane, and A. Kheddar, "Multi-character physical and behavioral interactions controller," *IEEE Transactions on Visualization and Computer Graphics*, vol. 23, no. 6, pp. 1650–1662, June 2017.

[11] K. Bouyarmane and A. Kheddar, "On weight-prioritized multi-task control of humanoid robots," *IEEE Transactions on Automatic Control*, 2018.

[12] V. Samy and A. Kheddar, "Falls control using posture reshaping and active compliance," in *IEEE-RAS International Conference on Humanoids*, Seoul, Korea, 2015, pp. 908–913.

[13] V. Samy, K. Bouyarmane, and A. Kheddar, "QP-based adaptive-gains control to lower damage in humanoid falls," in *IEEE International Conference on Robotics and Automation*, Singapore, 2017.

[14] T. Moulard, F. Lamiraux, K. Bouyarmane, and E. Yoshida, "Roboptim: an optimization framework for robotics," in *Robomec*, 2013, p. 4p.

[15] V. Samy, S. Caron, K. Bouyarmane, and A. Kheddar, "Adaptive Compliance in Post-Impact Humanoid Falls Using Preview Control of a Reduce Model," Jul. 2017, working paper or preprint. [Online]. Available: https://hal.archives-ouvertes.fr/hal-01569819

[16] K. Bouyarmane and A. Kheddar, "Fem-based static posture planning for a humanoid robot on deformable contact support," in *Humanoid Robots (Humanoids), 2011 11th IEEE-RAS International Conference on*. IEEE, 2011, pp. 487–492.